Carbon Dots for Super-resolution Imaging of Nanoporous Catalysts

Marissa van der Asdonk[†], Rafael Mayorga-Gonzalez[†], Yadolah Ganjkhanlou[†], and Florian Meirer[†]

[†] *Inorganic Chemistry & Catalysis (ICC), Debye Institute for Nanomaterials Science, Utrecht University, 3584 CG Utrecht, The Netherlands*

Key Words: Carbon dots - Fluorescence - Nanoprobe - Synthesis - Super-Resolution Imaging - Nanoporous catalyst

Abstract: Mass transport within the pore structure of a catalyst particle is a crucial factor in its catalytic efficiency. Therefore, studying the pore network of a catalyst is vital for rational catalyst design. One promising method for this is super-resolution fluorescence microscopy, which has the potential to localize fluorescent probes within pore spaces with an accuracy below the diffraction limit. In this work, we show that carbon dots based on citric acid and urea have great potential for pore space mapping with confocal laser scanning microscopy and single particle tracking using super-resolution fluorescence microscopy. Furthermore, it is possible to embed a molecular fluorophore, resorufin, inside the CDs for brighter luminescence than pure CDs and therefore enhanced particle localization/tracking. We synthesized and characterized two carbon dot samples using HRTEM, photoluminescence, UV-vis, infrared, and Raman spectroscopy techniques. With these results, we demonstrate that it is possible to use these carbon dots in super-resolution microscopy studies, paving the way for a future application of carbon dots in pore space exploration.

■ Introduction

Mass transport within a catalyst particle is an important and often limiting factor for the speed and efficiency of catalytic conversion.[1] Reactants need to reach the active sites inside the pore network while the products formed subsequently need to leave again to make way for new reactants. As mass transport is determined by the pore structure of a catalyst particle, a proper characterisation of its features and how they relate to synthesis parameters holds the key to designing better catalysts. A promising tool to map porosity is to track individual fluorescent probes as they diffuse within catalyst particles.

Carbon dots (CDs) are organic luminescent materials that could be used for this purpose. They were accidentally discovered by Xu et al. in 2004 as a byproduct of carbon nanotube purification and were shown to be bright fluorophores, photostable, economical, non toxic, and easy to synthesize.[2,3] Their photo-luminescent (PL) properties are the result of four different sources: carbon core state luminescence due to quantum confinement of the conjugated π-system, surface state luminescence emerging due to interactions between core state and surface groups, the cross-link enhanced emission effect, and luminescence of embedded fluorophores.[4–6] It has been shown that fluorophores such as citrazinic acid can be formed during the synthesis of CDs, and recent studies have shown that PL emission for CDs with high quantum efficiency originates mainly from luminescence of these embedded fluorophores.[7,8]Formation of fluorophores for similar reactions was reported as early as 1893 by Sell et al., who showed that citrazinic acid and 2-pyridone based fluorophores formed during the condensation reaction of CA with ammonia.[9]

CDs have been opted to be used as chemo-sensors to detect metal ions in various solvents and to get information about the local pH within biological systems, as different conditions cause different emission wavelengths.[10–12] Their use in catalyst pore-space mapping on the other hand has not been explored thoroughly. One technique that appears particularly promising to track the movement of CDs within catalyst pore spaces is super-resolution fluorescence microscopy (SRFM). This technique can localize fluorophores below the diffraction limit by using Gaussian fit localization over diffraction limited fluorescent spots. By following fluorophores over multiple frames, these molecules can be tracked in time and space. Although carbon dots have been used with super-resolution microscopy techniques by other research groups, the majority of these studies use CDs dried on a coverslip.[13–17] The use of moving CDs in super-resolution microscopy studies has not been reported.

In this Thesis, we track CDs in liquid using SRFM. We synthesized two types of CDs; one 'classic' CD with fluorescence stemming from embedded intermediate molecules, and a CD with extra fluorescent dye, resorufin, embedded in it. A total of five CD samples were synthesized (Table S1), however, we will only be focusing on the most promising CD sample for each group. We characterized the CDs concerning their functional groups, their relative quantum yield, their size, and their crystallinity both in the bulk sample and on the single particle level. We then conducted a study to find conditions at which our CDs portrayed minimal adsorption on porous silica particles using Confocal Laser Scanning Microscopy (CLSM). The absence of adsorption events is necessary for efficient particle tracking, as a particle standstill caused by adsorption will

complicate pore space mapping. Lastly, we showed that it was possible to track individual CDs as they diffused in free solution, which allowed us to determine their size distribution. Collectively, this work paves the way for a future application of CDs in pore space exploration using SRFM.

■ Methods

Carbon Dot Synthesis. The synthesis of the CDs was conducted via an adaptation of the protocol by Strauss et al..[18] A visual representation of the synthesis is described in Figure 1a. CA monohydrate and urea was added to a vial in a 1:2 ratio (w/w). Resazurin dye was added to the first sample in the same ratio as CA, this molecule is reduced to the fluorescent resorufin due to the presence of urea; this sample will further be referred to as CU250-R, as short for CA mixed with Urea, heated to 250 °C, with embedded Resorufin. A magnetic stirrer was added to the vial, and it was placed in an aluminium reaction block on top of a hot plate. The hot plate was programmed to heat up to 250 °C using a compatible thermometer, at which the temperature was kept for 15 minutes. The second sample was prepared using 5 ml formamide (FA) as a solvent. The mixture was poured in a Teflon-lined autoclave (Parr 4749). To prevent high pressure build-up, the temperature for this sample's solvo-thermal synthesis was reduced to 180 °C. Due to the lower temperature, the timescale for the CD formation was increased to three hours. This sample will further be referred to as CU180-FA, as short for CA mixed with Urea, heated to 180 °C, prepared using FA as a solvent. Due to the use of a non-aqueous solution, we expect the CDs in this sample to have an amphipathic character and a more uniform morphology compared to the CDs in the sample prepared by solid state pyrolysis.

Once the samples were cooled down to room temperature, CU250-R was dissolved in water. Both samples were subsequently filtered through a 0.2 μm PFTE filter and poured into a dialysis membrane (high retention seamless cellulose tubing (MWCO 12.4kDa, Sigma-Aldrich)). Dialysis was performed for one week, where the dialysate was disposed of and replaced with fresh deionized water on a daily basis. Before disposal, the dialysate was checked for presence of luminescence with a 405 nm laser pointer (5 mW). A week was chosen as dialysis endpoint as the concentration of luminescent molecules in the dialysate was no longer observable by the human eye at this point. This dialysis process ensured that any small molecules such as individual fluorophores or reactants were filtered out.

Embedding of resorufin. In order to determine whether or not we were successful in embedding resorufin inside the CDs for the CU250-R sample, UV-vis spectra were recorded of the CD solution. The spectra were recorded at room temperature using a UV-CARY 200 spectrophotometer. The embedding of resorufin will furthermore be verified using other techniques discussed in the coming sections.

Fluorescent properties. Photoluminescence emission spectra were recorded with a Jasco spectrofluorometer (FP 8300) at 200 nm/min. Emission spectra were gathered using varying excitation wavelengths between 350 and 600 nm, while emission intensity values were collected at wavelengths 10 nm above the excitation wavelength up until 750 nm.

Quantum Yield. If you plot the absorbance versus the fluorescence of different concentrations of a sample, this formula can be used to estimate the QY:[19]

$$\Phi_x = \Phi_{\text{std}} \left(\frac{\text{slope}_x}{\text{slope}_{\text{std}}} \right) \left(\frac{\eta_x}{\eta_{\text{std}}} \right)^2 \quad (1)$$

In this equation, Φ_x and Φ_{std} denote the relative QY of the sample and reference fluorophore respectively. Slope_x and slope_{std} represent the slope of the regression line. Lastly, η is the refractive index.

Rhodamine B was chosen as a reference sample as it is well studied and has a similar excitation and emission region, ensuring a good relative QY calculation. The regression line for the rhodamine B was obtained by averaging the absorbance for 550-555 nm and plotting out the result against the fluorescence averaged over 570-575 nm for 4 samples with varying low concentrations. This process was repeated for the CD samples and the non-embedded molecular fluorophore resorufin.

Functional Groups. Furthermore, micro fourier-transform infrared (μ-FTIR) spectra were measured using a Perkin Elmer FTIR in attenuated total reflectance mode. Samples were prepared by drying a droplet (volume = 10 μl) of sample on a CaF_2 disk. FTIR spectra were collecting in transmittance mode, compared to each others, and peaks were clarified using IR tables.[20,21]

Crystallinity. Both single particle and bulk crystallinity were studied using High-Resolution Transmission Electron Microscopy (HRTEM) and Raman spectroscopy, respectively.

HRTEM images of CD samples were collected with a TALOS F200x Transmission Electron Microscope. Samples were prepared by pipetting 5 μl sample on a TEM grid (formvar on 3mm, 300 mesh Cu grid) and leaving the sample to dry under a clean glass beaker. Thereafter, the grid containing the sample was placed in the sample holder and imaged at 390kx magnification.

Raman spectra were qcquired using a Renishaw Invia Raman microscope equipped with a 785 nm laser, the power at the sample was $\sim$0.22 mW. Measurements were done with a 1200 l/mm grating, 50x objective, and 10 s acquisition time. Spectra were collected for CU180-FA and CU250-R. Additionally, a spectrum for graphite was collected as a reference, since it is expected that CDs have a similar crystalline structure to Graphite.[24] For the CD samples, we dried some drops

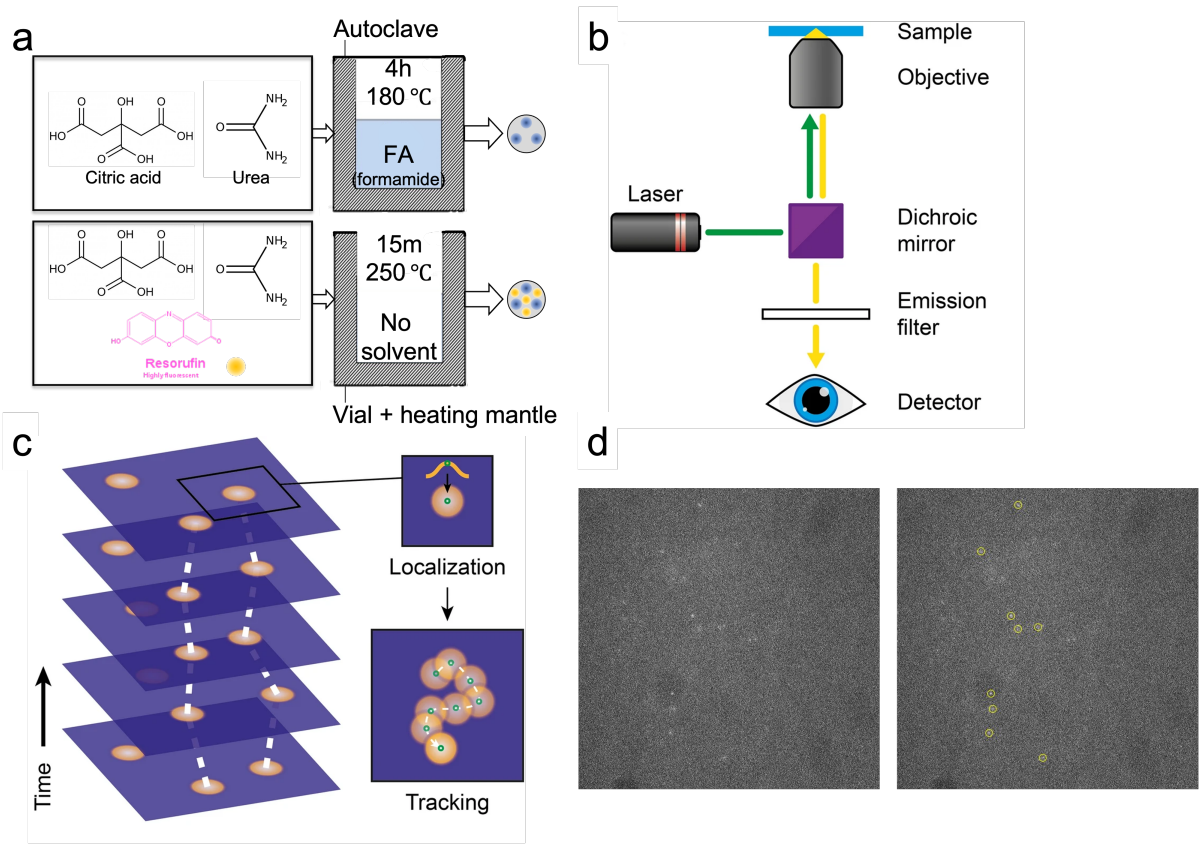

Figure 1: **Schematic representation of CD synthesis methods used in this paper, fluorescence microscopy, and particle tracking, and visualisation of Gaussian fit localization using the ImageJ DOM plugin.** (a) Schematic of the synthesis of CDs used in this research. First CD sample was prepared via solvothermal synthesis of citric acid and urea using formamide as a solvent. This synthesis was carried out in an autoclave at 180 °C for 4 hours. The second CD sample was also prepared via solvothermal synthesis of citric acid and urea, but resazurin was added. This synthesis was carried out in a vial in a heating mantle at 250 °C for 15 minutes without a solvent. (b) Schematic representation of a wide field fluorescence microscope set-up consisting of an excitation source (laser), dichroic mirror, obective lens, filter, and detector. The laser light (green) is reflected onto the sample via the dichroic mirror through an objective, but fluorescent light emitted by the sample (yellow) is let through and collected by the detector. Adapted from Maris et al.[22] (c) Single particle tracking of individual emitters, which will be observable as diffraction-limited spots, can be done by Gaussian fit localization. Individual localizations over multiple frames are then grouped together in a trajectory, which can then be interpreted. Adapted from Maris et al.[22] (d) Single frame example of Gaussian fit localization of resorufin embedded CDs in free solution (15/85 water/glycerol) using the ImageJ DOM plugin.[23] CD particles visible as diffraction-limited spots (left), and localized CD particles (right).

of CD solution on a glass coverslip to obtain a solid layer of particles. The graphite sample was measured from a solid graphite piece obtained from a pencil.[25]

CD adsorption behaviour tunability. Since adsorption is detrimental for pore space exploration using SPT, we carried out a preparatory study in which we attempted to find electrostatic conditions in which our CDs diffuse into a porous silica model system with minimal adsorption on pore walls. This study was conducted using CLSM.

Microscope slides were prepared by first applying a Thermo Scientific^{TM} 25 μl Gene Frame (AB0576) on a thin objective glass. Then, a small amount of porous silica spheres ($\sim$20 μm diameter, pore size $\sim$35 nm) were added inside the Gene Frame. Lastly, 4 μl of CDs and 18 μl of buffer was added to the Gene Frame before closing it with a coverslip. The prepared slides were then left to equilibrate for 2 weeks before being measured.

Slides were assembled containing either CU250-R or CU180-F adding pH buffer of pH 4, 7, or 10. Moreover, one last slide was prepared for each CD sample with pH 7 buffer,

but replacing part of the buffer with a salt solution such that we end up with a 0.01M NaCl solution.

CLSM images of the silica particles containing CDs were collected using a Nikon A1 inverted microscope with 405, 488, 566, and 635 nm lasers. An average fluorescent intensity outside of the silica particles was subtracted from the intensity found inside of the silica particles to give an indication of the CD concentration inside the silica particles. A positive value in this case indicates a higher CD concentration inside the silica particles, which we would expect to be due to adsorption. We used the data from the 468 nm laser and the 405 nm laser channel for CU250-R and CU180-FA, respectively. The channels were chosen based on intensity values being high enough for a good signal-to-noise ratio (SNR) without overloading the detector.

Super-resolution Fluorescence Microscopy study. To conclude this work, a SRFM study was conducted in order to investigate whether individual CDs could be localized and tracked with SRFM. As it was a proof-of-principle study, only CU250-R was used in the SRFM studies. One crucial step to achieve localization and tracking was to dilute the chosen CU250-R CD samples with an 85/15 glycerol/water solution. This water/glycerol mixture served a dual purpose. Firstly, it matches the refractive index of the solution to that of the glass coverslip to increase the signal-to-noise ratio. Secondly, it slows the CDs down by increasing the viscosity of the solvent compared to a water solution. Slowing the CDs down is important because the diffusion speed of the particles will be too fast to track with our SRFM setup due to the very small size of the CDs.

To prepare the samples, we place a Thermo Scientific™ 25 μl Gene Frame (AB0576) on top of a plasma cleaned coverslip. Meanwhile, the vial with CDs was placed in an ultrasonic bath for 15 minutes to reduce aggregates. Then, the CDs were diluted 100x using an 85/15 solution of glycerol/water so that 22 μl of diluted sample was pipetted inside the Gene Frame. We closed the Gene Frame using a provided coverslip, and placed the sample inside of the sample holder of the microscope. Measurement was done with all external lights turned off to decrease noise, and 500 frames worth of measurement was collected.

Once complete, the data was analyzed using imageJ with the DoM plugin.[23] The plugin is first used to detect the location of the molecules in each of the frames, as shown in Figure 1d. Once particles were localized over several frames, multiple localizations that most likely belonged to the same particle were linked together, forming tracks. These tracks were then visualised as can be seen in Figure 4d. This data is the basis for the size distribution calculations described earlier.

Size determination. In order to determine the size of our CDs, we first attempted this with dynamic light scattering (DLS). However, these measurements did not yield any useful results. The first reason for this is that the refractive index of carbon is not much different from that of water, which greatly decreases the SNR. The SNR further decreases because the fluorescent light emitted by the CDs interferes with the signal of the scattered light. Lastly, we know that the CDs show at least some degree of aggregation; as this technique is most sensitive to large particles, the results become even more unreliable.

The size was later successfully estimated using HRTEM with the same parameters as described for the determination of crystallinity. Furthermore, a size distribution was calculated using SRFM. Mean square displacement (MSD) values, $\mathrm{MSD} = \langle (x(t) - x_0)^2 \rangle$, were calculated for each track and related to a diffusion coefficient (D) by plotting the MSD as a function of the time-delay $MSD(t) = a + bt$ and using the function $D = b/4$.[26] With this data, we can calculate a size distribution by using the Stokes-Einstein equation

$$R_0 = \frac{k_B T}{6\pi\mu D} \tag{2}$$

in which k_B is the Boltzmann's constant, T is the temperature in K, μ is the solvent viscosity, and R_0 is the radius of the tracked particle. Doing this for each track gave us a size distribution for the particles in our sample.

Materials. Urea (purity 99.5%, Sigma-Aldrich), Citric acid monohydrate (purity 99.0%, Sigma-Aldrich), Formamide (purity $\geq$ 99%, brand), Resazurin sodium salt (Sigma), Potassium phosphate monobasic (purity $\geq$ 99.5%, Sigma-Aldrich), Potassium phosphate dibasic trihydrate (purity $\geq$ 99.0%, Sigma-Aldrich), Dialysis tubing, high retention seamless cellulose tubing (MWCO 12.4kDa, Sigma-Aldrich), VWR 0.2 μm PTFE filter.

■ Results and Discussion

When comparing the UV-vis spectra of CU180-FA and CU250-R, as depicted in Figure 2a and Figure 2d respectively, we observe quite similar electron transitions. In both spectra we see C=C $\pi - \pi*$ electron transitions, C=O n-$\pi*$ transitions, and C=N transitions.[27] Interestingly, an extra absorbance peak is observed for the CU250-R sample at 571 nm. This peak corresponds to the wavelength at which resorufin shows the highest absorption according to both literature and our own UV-vis measurements (Figure S1).[28] This is a strong indicator that we have managed to embed resorufin inside our CU250-R CDs, as non-embedded molecular resorufin would have been filtered out by the dialysis process due to its small size (0.7 nm).[29]

In order to get a clear view of the photoluminescent behaviour of our samples, the curves for each excitation wavelength were overlaid. When doing this, we observe an excitation dependent emission for the CU180-FA CDs in Figure 2b.

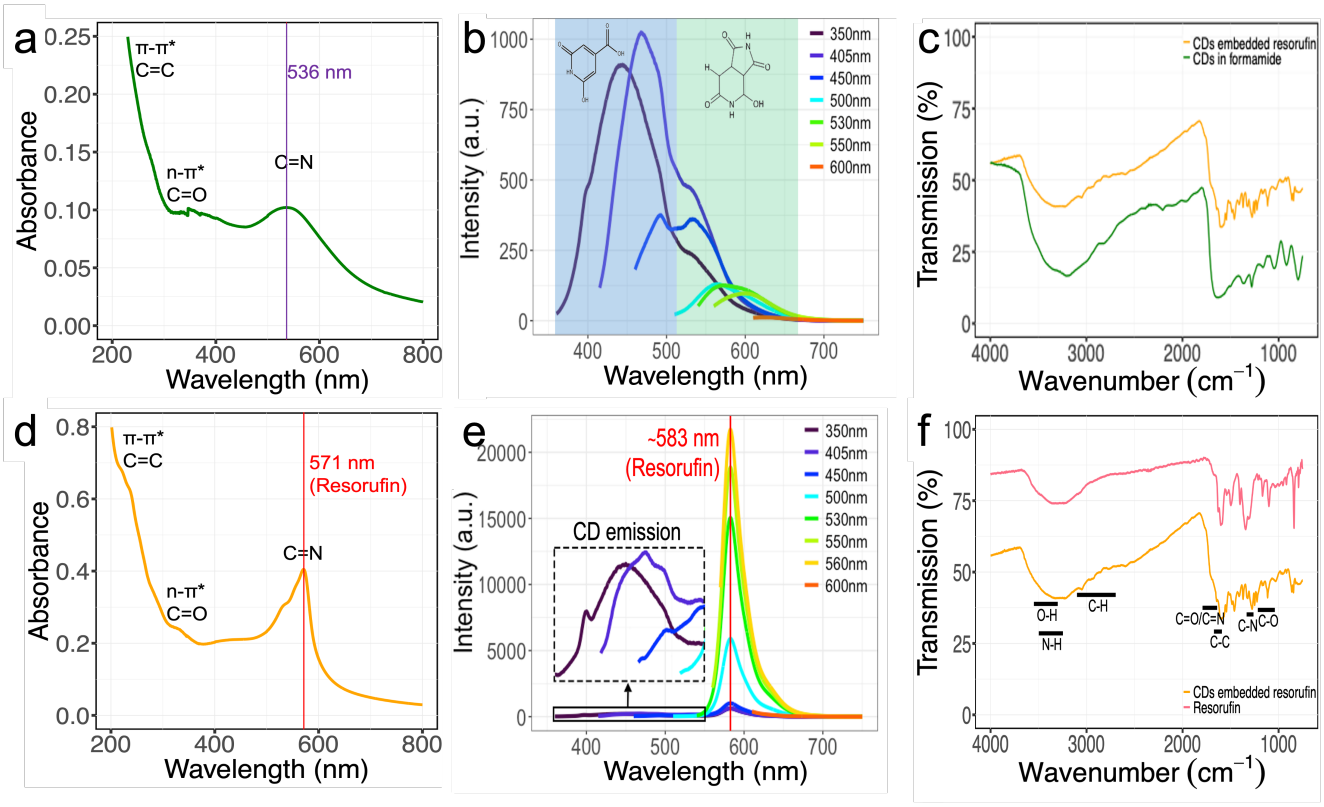

Figure 2: **UV-vis, Photoluminescence, and FTIR characterization spectra of CDs prepared in formamide (CU180-FA) and CDs embedded with resorufin (CU250-R).** (a) The UV-vis spectrum of CU180-FA shows the $\pi - \pi*$ electron transitions of C=C, the n-$\pi*$ of C=O and C=N. (d) The UV-vis spectrum of CU250-R shows these same electron transitions, but has an additional peak at 571 nm, corresponding to the excitation peak of resorufin. (b) The Photoluminescence spectrum of CU180-FA shows an excitation dependent emission. The left group of peaks are expected to be present due to the formation of blue emissive citrazinic acid and similar single aromatic fluorophores. The right group of peaks are expected to be present due to the formation of green emissive species with two or more aromatic ring fluorophores such as hydroxy-1H-pyrrolo[3,4-c]pyridine-1,3,6(2H,5H)-trione (HPPT) and similar structures. (e) In comparison, the photoluminescence spectrum of CU250-R shows a similar excitation dependent emission, but additionally displays a dominant luminescence peak at 583 nm, corresponding to the emission of resorufin. (c) When comparing the FTIR spectra of the CD samples, we observe similar peaks, but the spectrum for CU180-FA shows a broader peak around 1800 cm^{-1}. (f) Comparing CU250-R with molecular resorufin, an extra peak is observed for the CDs at approximately 3000 cm^{-1}.

This excitation dependent emission behaviour was expected, as it is commonly reported about in literature.[7,8,30] In these excitation dependent emission peaks, we can observe two sets of peaks. There are multiple conflicting mechanisms reported for the origin of this excitation dependent mechanism, some of which would indicate a deviation from Kasha's; a rule which describes that a fluorophore only emits light from its lowest energy excited state. These mechanisms include the presence of different fluorophores, aggregation, or CD heterogeneity.

A group of blue-emissive fluorophore peaks can be observed around 460 nm; these could be allocated to fluorophores with single aromatic rings such as citrazinic acid or similar molecules.[7,8,31] Moreover, a group of green emissive fluorophore peaks can be observed around 550 nm. This group of peaks could be allocated to fluorophores with two or more aromatic rings such as hydroxy-1H-pyrrolo[3,4-c]pyridine-1,3,6(2H,5H)-trione (HPPT) and similar molecules.[31] A similar excitation dependent emission was observed for CU250-R, as can be seen in Figure 2e. Additionally, we observe a dominant luminescence peak at 583 nm. Contrary to the others, this peak does not show excitation dependent emission behaviour, indicating its origin to be a single fluorophore. Furthermore, this peak's wavelength corresponds to the emission of resorufin as described in literature, thus further substantiat-

ing our claim that we have indeed embedded resorufin inside of our CDs.[28,32]

By combining data from UV-vis and Photoluminescence, we were able to calculate a relative quantum yield for both our CDs and molecular resorufin dye. For this, we compare the samples to a known sample of Rhodamine B, which has a QY of 0.31 in water.[33] Calculations were conducted using Equation 1, absorbance-fluorescence plots can be found in Figure S3 and Figure S2, and calculated results are displayed in Table 1.

Table 1: Overview of quantum yield of known fluorophore Rhodamine B and therewith calculated relative quantum yields for CDs embedded dye (CU250-R), CDs in FA (CU180-FA), and resorufin molecular fluorophore. *: Excitation maximum for Rhodamine B was 554 on used instrument.[33]

Sample name	$\lambda_{ex}(nm)$	Quantum Yield
Rhodamine B	554*	0.31
CDs in FA	560	0.201
CDs embedded dye	560	0.175
Resorufin	560	0.204

We found a relative QY of 0.201 for CU180-FA. Surprisingly, we calculated a lower relative QY of 0.175 for CU250-R, also lower than the relative QY for molecular resorufin which was calculated to be 0.204. A possible explanation for this could be that the fluorescence for CU250-R comes mainly from embedded resorufin, which may lose QY due to more non-radiative decay due to being surrounded by carbon structures.[34]

When comparing the FTIR spectra of the CD samples, as shown in Figure 2c, similar bands are observed. However, one notable difference between the two graphs is that there is a broader and more pronounced band visible for the CU180-FA CDs around 1800 cm^{-1} compared to the CU250-R CDs. As this region indicates C=O/C=N bonds, we expect this difference to be due to an increased presence of nitrogen containing species in CU180-FA. Furthermore, we compared CU250-R to resorufin in its molecular form, seen in Figure 2f, we see that an extra band is observed for the CDs at approximately 3000 cm^{-1}. A band in this region is indicative of the presence of more carbon, something that is in line with our expectations of resorufin being embedded inside of a CD structure.

HRTEM images of the CD samples were collected in order to study the internal structure and crystallinity. With this, we were able to observe crystal lattice fringes in both CU180-FA and CU250-R samples. Looking at the HRTEM image of CU180-FA, as shown in Figure 3a, we observed an aggregate of CDs showing a small crystalline domain in the middle. The d-spacing of this crystalline domain was calculated to be 6.25 ± 1.24 $\AA$. The HRTEM image for CU250-R, Figure 3b, showed aggregation even more clearly. When zooming in to a small part of this image (Figure 3c), we could again observe crystal lattice fringes clearly with large and smaller domains. When plotting a gray value plot of the yellow highlighted cross-section over the lattice fringes, as depicted in Figure 3d, we calculated the d-spacing to be 3.18 ± 0.16 $\AA$. A similar lattice spacing (0.302 nm) for comparable CDs was observed by Liu et al. (2014).[35] Furthermore, the (002) lattice plane of graphite is reported to be 3.36 $\AA$ in literature.[36,37]

After observing crystallinity in individual CD particles, we used Raman spectroscopy to study this property in bulk sample. Spectra were normalized and overlaid in one figure so that a proper comparison could be made. The Raman spectra of CU180-FA, CU250-R, and a graphite reference are depicted in Figure 3e. Here, we see that both CD samples show peaks around the D (disordered carbon) and G (ordered, sp^2 carbon) band of graphite, indicating the presence of both crystalline and disordered carbon structures in the CD samples.[38] Furthermore, we observe a notable peak to the left side of the D band for CU180-FA. A shift to the left for the D band is an indication of an increased presence of N-doped species.[38]

Combining the previously discussed data, we can estimate the resulting morphology of our two CD samples. As seen in Figure 3f, CU180-FA is expected to have some smaller crystalline C domains with relatively large d-spacing. Trapped within these carbon domains are fluorescent species similar to citrazinic acid and HPPT. In contrast, CU250-R is shown in Figure 3g which portrays more and larger crystalline C domains with a much smaller d-spacing. Trapped within these CDs are the same fluorescent species similar to citrazinic acid and HPPT, but additionally there are resorufin fluorophores embedded.

In order to accurately map pore spaces using SPT, it is necessary to find a combination of host, probe and solvent conditions where adsorption does not take place. For this reason, we first conducted a preparatory study using CLSM to find these conditions. An example of a CLSM image of a porous silica particle stained with CDs is shown in Figure 4e. First looking at CU180-FA, as seen in Figure 4a, we observe a positive intensity for all of the conditions (pH = 4, 7, 10; Ionic strength = 25 mM. Schematic of expected interactions between silica pore walls and CDs is shown in Figure S5) that were explored. As this displayed intensity is the result of subtracting the average intensity outside the particles from the average intensity in each particle, this indicates an overall higher fluorescence concentration coming from within the particle. This increased fluorescence concentration from within the particles is due to an increased concentration of CDs due to adsorption of the CDs on the pore walls. Therefore, we did not find a suitable condition for the CU180-FA CDs at which they had minimal adsorption on the silica. Interestingly the CU250-R sample

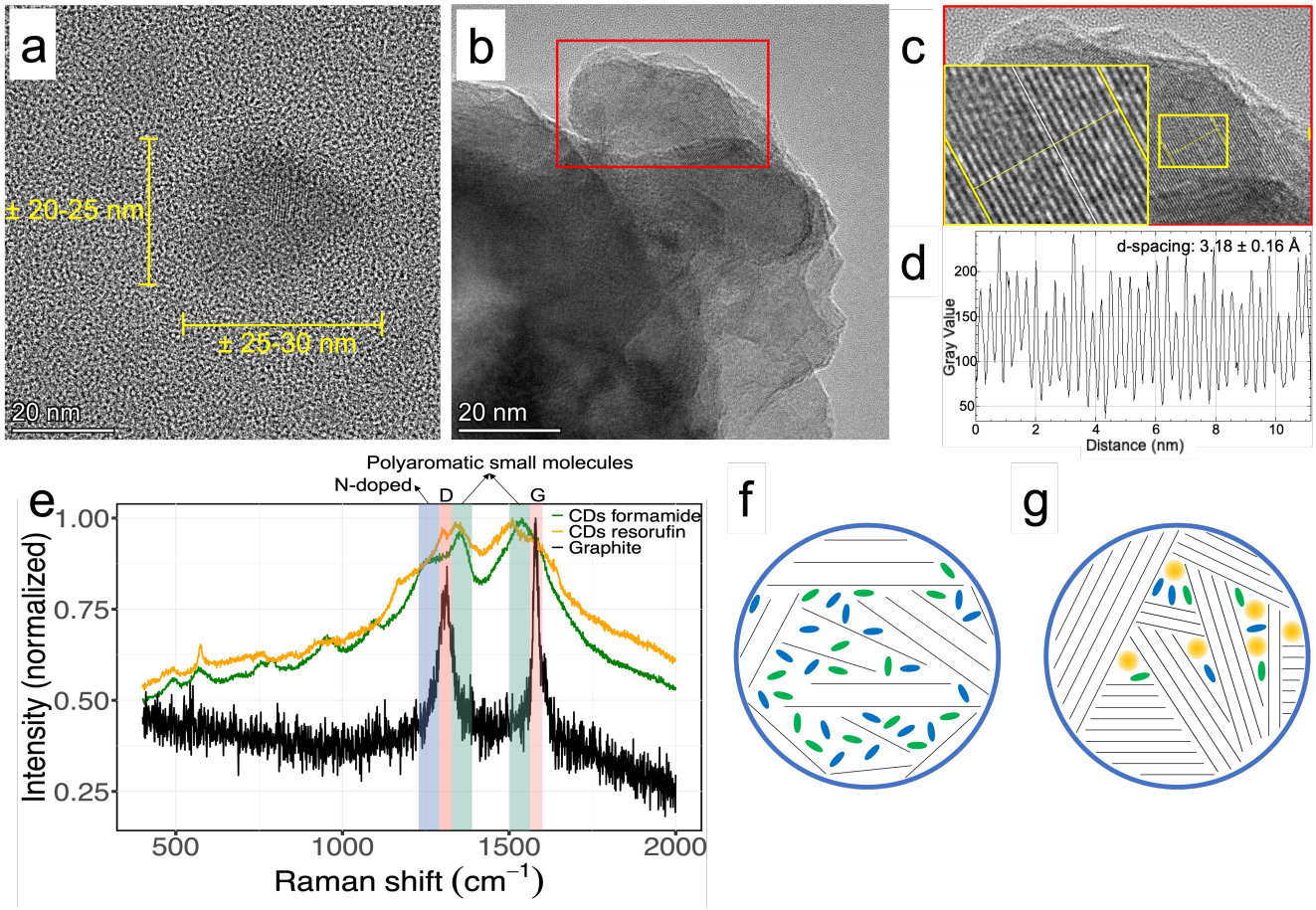

Figure 3: **HRTEM images, Raman spectra, and a schematic representation of the synthesized CDs.** (a) HRTEM image (390 kx zoom) of CDs prepared in formamide (CU180-FA), CDs are likely clustered. A small crystalline domain is observable which was found to have a d-spacing of 6.25 $\pm$ 1.24 $\mathring{A}$. (b) HRTEM image (390 kx zoom) of CDs with embedded resorufin (CU250-R), clustering observable. (c) Zoomed in image of b) showing clear lattice fringes. (d) Gray value plot of the yellow highlighted cross-section over the lattice fringes in c). Averaging over these spacings, a d-spacing of 3.18 $\pm$ 0.16 $\mathring{A}$ is found. (e) Raman spectra of CU180-FA, CU250-R, and graphite for reference. Peaks are observed for both CD samples around the D (disordered) and G (ordered) band of graphite, indicating the presence of crystallinity in bulk. (f) Schematic representation of CU180-FA according to the information gathered from characterization, some crystalline domains with relative large spacing and embedded fluorescent species. (g) Schematic representation of CU250-R according to characterization, large crystalline domains with smaller spacing and presence of embedded resorufin in addition to the other fluorescent species.

showed different behaviour, as shown in Figure 4b. A lower pH (pH = 3.97) shows an overall higher intensity compared to the neutral or basic pH, most likely caused by adsorption. We expect our silica to always be negatively charged for the measured pH values ($\geq$ pH 4).[39,40] Increasing the pH then increases the repulsion between the silica host and the CD probes, resulting in a decrease in adsorption to the pore wall and CD aggregation. In the condition where salt ($\sim 0.01M$) was added, fluorescence was also increased inside the particles compared to outside. This can be explained due to a decrease in Debye length as a result of the introduced ions, allowing the CDs to get closer to the silica surface which in turn increases adsorption. Under these conditions the repulsive electrostatic forces between the CDs are also screened, resulting in CD aggregation (see Figure S4). Interestingly, basic pH (pH = 10.0) seems to generally exhibit an intensity inside the particles that is similar to or lower than the fluorescence outside of the particle, indicating minimal adsorption of the CDs on the pore walls. The tunability of the adsorption behaviour of the resorufin-embedded CDs makes it a promising probe

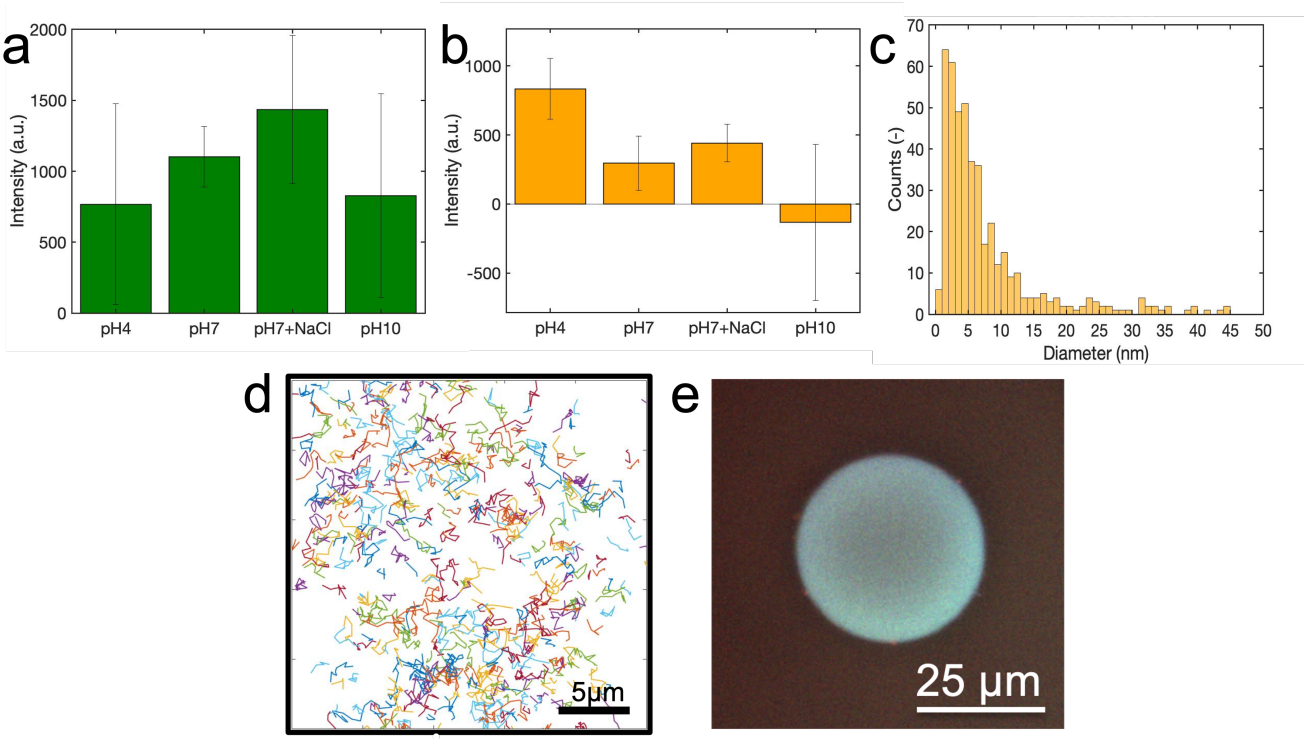

Figure 4: **Confocal Laser Scanning Microscopy prepaparation study, size distribution graphs, SPT tracks, and stained porous silica particle; error bars indicate the deviation between particles within a sample.** (a) CLSM graph of porous silica spheres (size $\sim$20 μm, pore size $\sim$ 35nm) stained with CDs prepared in formamide (CU180-FA). Shown is the fluorescent intensity outside the silica particle subtracted from the intensity inside the particle. In all conditions, more fluorescence is observed inside the silica particle than outside. (b) CLSM graph of porous silica spheres stained with CDs with embedded resorufin (CU250-R). An overall lower fluorescent intensity is observed for pH10 condition. (c) Size distribution graph for CU250-R, calculated from SRFM particle tracking data. (d) Visualisation SPT tracks of CU250-R in porous silica. (e) CSLM image of a porous silica particle stained with CDs.

to map the pore space of porous silica particles with single particle tracking. Of note, the solubility of silica is known to rapidly increase at pH values above 9, which potentially influences our results.[41] Therefore, these experiments should be repeated at pH values between 7 and 9.

Lastly, we tracked CU250-R in a water glycerol solution using a widefield fluorescence microscope (see Figure 1d). By performing a MSD analysis of the individual tracks, (visualised in Figure 4e) we obtained single particle diffusion coefficients which were translated into particle sizes (see Figure 4c) with the Stokes-Einstein equation (Equation 2). Most of the CDs showed a diameter of approximately 5 nm. However, larger particles (15-45 nm), possibly clusters, were observed as well. Due to the lack of uniformity in the particle size distribution, dynamic light scattering could not provide a measurement for CD size. This highlights the potential of SPT not only as a way to characterize porous materials, but also to characterize the size of CD probes.

■ Conclusion

We were able to embed the molecular fluorophore resorufin inside CDs by adding resazurin before the synthesis, which reduces to the fluorescent resorufin. We found a CD sample, the CDs with embedded resorufin, that was very promising for pore space mapping with SPT using SRFM. This sample showed bright fluorescence and could be tuned to absorb less on the pore walls of porous silica.

Moreover, it was possible to track the synthesized CDs with embedded resorufin using SRFM, and this data was used to estimate their size distribution. The CD size distribution was found to be heterogeneously distributed, with most particles having a diameter of $\pm$ 5 nm. More common methods for size distribution estimation, such as DLS, did not result in reliable measurements, showing the added value of using SRFM.

A relative quantum yield of $\pm$ 17% and $\pm$ 20 % was found for the CDs with embedded resorufin and the CDs prepared in

formamide respectively.

Finally, our findings have shown that the aggegation status and adsorption of CDs on pore walls depend on the pH of the environment and the increased presence of ions in the form of added NaCl. Both an acidic pH and introduction of NaCl showed to increase aggregation and adsorption. For the porous silica model system we used, a basic pH showed to be most promising for future studies.

■ Future outlook

Our aspirations for these carbon dots are to use them for mapping the complicated pore structure of catalyst particles. Although we have shown it possible to track these CDs with SRFM, it is important that this work will first be expanded towards a study within a porous model material such as the porous silica beads that we used in the CLSM study. For this, we would advice using a slightly basic solution with a pH value between 7 and 9. After these studies, experiments should be aimed towards exploring different surfaces so that it can eventually be used for pore space exploration.

■ Acknowledgements

First of all, we would like to thank all ICC members for their support, scientific discussions and any contributions they have made to make this thesis possible.

Furthermore, I, Marissa van der Asdonk, would personally like to thank Rafael Mayorga-Gonzalez and Yadolah Ganjkhanlou for their excellent supervision of my master thesis project.

I would also like to thank the Pore Space Exploration pillar group members, Florian Meirer, Rafael Mayorga-Gonzalez, Yadolah Ganjkhanlou, Erik Maris, Joren Dorresteijn, Caroline Versluis, Bettina Baumgartner, Justin Heesakkers, Alessia Broccoli, and Luca Carnevale for the weekly meetings and discussions.

Lastly, I would like to thank Angela Melcherts for her support with HRTEM measurements, Adriaan Duijndam for his support with DLS measurements, Joris Koek for his support with TEM measurements, and Sanne Kers for allowing us to measure UV-vis and Photoluminescence on their equipment.

References

1 Trogadas, P., Nigra, M. M. & Coppens, M. O. Nature-inspired optimization of hierarchical porous media for catalytic and separation processes. *New Journal of Chemistry* **40**, 4016–4026 (2016).

2 Xu, X. *et al.* Electrophoretic analysis and purification of fluorescent single-walled carbon nanotube fragments. *Journal of the American Chemical Society* **126**, 12736–12737 (2004).

3 Sim, L. C. *et al.* Carbon dots synthesized from green precursors with an amplified photoluminescence: Synthesis, characterization, and its application. *Nanotechnology in the Life Sciences* 1–33 (2019).

4 Xiong, Y., Schneider, J., Ushakova, E. V. & Rogach, A. L. Influence of molecular fluorophores on the research field of chemically synthesized carbon dots. *Nano Today* **23**, 124–139 (2018).

5 Xia, C. *et al.* Evolution and synthesis of carbon dots: From carbon dots to carbonized polymer dots. *Advanced Science* **6**, 1901316 (2019).

6 Dhenadhayalan, N., Lin, K. C., Suresh, R. & Ramamurthy, P. Unravelling the multiple emissive states in citric-acid-derived carbon dots. *Journal of Physical Chemistry C* **120**, 1252–1261 (2016).

7 Zhu, S., Zhao, X., Song, Y., Lu, S. & Yang, B. Beyond bottom-up carbon nanodots: Citric-acid derived organic molecules. *Nano Today* **11**, 128–132 (2016).

8 Kasprzyk, W., Bednarz, S., Zmudzki, P., Galica, M. & Bogdał, D. Novel efficient fluorophores synthesized from citric acid. *RSC Advances* **5**, 34795–34799 (2015).

9 Sell, W. J. & Easterfield, T. H. LXXIII. - Studies on citrazinic acid. Part I. *Journal of the Chemical Society, Transactions* **63**, 1035 – 1051 (1893).

10 Yoo, D., Park, Y., Cheon, B. & Park, M. H. Carbon dots as an effective fluorescent sensing platform for metal ion detection. *Nanoscale Research Letters* **14** (2019).

11 Yarur, F., Macairan, J. R. & Naccache, R. Ratiometric detection of heavy metal ions using fluorescent carbon dots. *Environmental Science: Nano* **6**, 1121–1130 (2019).

12 Gao, X., Du, C., Zhuang, Z. & Chen, W. Carbon quantum dot-based nanoprobes for metal ion detection. *Journal of Materials Chemistry C* **4**, 6927–6945 (2016).

13 He, H. *et al.* High-density super-resolution localization imaging with blinking carbon dots. *Analytical Chemistry* **89**, 11831–11838.

14 Zhi, B. *et al.* Malic acid carbon dots: From super-resolution live-cell imaging to highly efficient separation. *ACS Nano* **12**, 5741–5752 (2018).

15 Wang, Q. *et al.* Nonblinking carbon dots for imaging and tracking receptors on a live cell membrane. *Chemical Communications* **57**, 5554–5557 (2021).

16 Khan, S., Verma, N. C., Chethana & Nandi, C. K. Carbon dots for single-molecule imaging of the nucleolus. *ACS Applied Nano Materials* **1**, 483–487 (2018).

17 Leménager, G., Luca, E. D., Sun, Y. P. & Pompa, P. P. Super-resolution fluorescence imaging of biocompatible carbon dots. *Nanoscale* **6**, 8617–8623 (2014).

18 Strauss, V., Wang, H., Delacroix, S., Ledendecker, M. & Wessig, P. Carbon nanodots revised: The thermal citric acid/urea reaction. *Chemical Science* **11**, 8256–8266 (2020).

19 Williams, A. T. R., Winfield, S. A. & Miller, J. N. Relative fluorescence quantum yields using a computer-controlled luminescence spectrometer. *Analyst* **108**, 1067–1071 (1983).

20 Ir spectrum table - merck. URL `https://www.sigmaaldrich.com/NL/en/technical-documents/technical-article/analytical-chemistry/photometry-and-reflectometry/ir-spectrum-table`.

21 Infrared spectroscopy absorption table - chemistry libretexts. URL `https://chem.libretexts.org/Ancillary_Materials/Reference/Reference_Tables/Spectroscopic_Reference_Tables/Infrared_Spectroscopy_Absorption_Table`.

22 Maris, J. J. E., Fu, D., Meirer, F. & Weckhuysen, B. M. Single-molecule observation of diffusion and catalysis in nanoporous solids. *Adsorption* (2021).

23 Katrukha, E. Detection of molecules (dom) plugin for imagej, v1.2.1. *Zenodo* (2020).

24 Mintz, K. J. *et al.* A deep investigation into the structure of carbon dots. *Carbon* **173**, 433–447 (2021).

25 Ritter, S. What's that stuff? Pencils & pencil lead. *Chemical and Engi-*

neering News **79**, 35 (2001).

26 Michalet, X. Mean square displacement analysis of single-particle trajectories with localization error: Brownian motion in an isotropic medium. *Physical Review E - Statistical, Nonlinear, and Soft Matter Physics* **82**, 041914 (2010).

27 Cui, L., Ren, X., Sun, M., Liu, H. & Xia, L. Carbon dots: Synthesis, properties and applications (2021).

28 Bueno, C. *et al.* The excited-state interaction of resazurin and resorufin with aminesin aqueous solutions. photophysics and photochemical reaction. *Photochemistry and Photobiology* **76**, 385–390 (2002).

29 Brühwiler, D., Gfeller, N. & Calzaferri, G. Resorufin in the channels of zeolite l. *Journal of Physical Chemistry B* **102**, 2923–2929 (1998).

30 Sharma, A. *et al.* Origin of excitation dependent fluorescence in carbon nanodots. *Journal of Physical Chemistry Letters* **7**, 3695–3702 (2016).

31 Kasprzyk, W. *et al.* Luminescence phenomena of carbon dots derived from citric acid and urea – a molecular insight. *Nanoscale* **10**, 13889–13894 (2018).

32 Grimm, J. B., Heckman, L. M. & Lavis, L. D. The chemistry of small-molecule fluorogenic probes. *Progress in Molecular Biology and Translational Science* **113**, 1–34 (2013).

33 Arbeloa, T. L., Arbeloa, F. L., Bartolomé, P. H. & Arbeloa, I. L. On the mechanism of radiationless deactivation of rhodamines. *Chemical Physics* **160**, 123–130 (1992).

34 Zu, F. *et al.* The quenching of the fluorescence of carbon dots: A review on mechanisms and applications. *Microchimica Acta* **184**, 1899–1914 (2017).

35 Liu, N. *et al.* One-step catalase controllable degradation of c3n4 for n-doped carbon dot green fabrication and their bioimaging applications. *Journal of Materials Chemistry B* **2**, 5768–5774 (2014).

36 Hayes, W. I., Joseph, P., Mughal, M. Z. & Papakonstantinou, P. Production of reduced graphene oxide via hydrothermal reduction in an aqueous sulphuric acid suspension and its electrochemical behaviour. *Journal of Solid State Electrochemistry* **19**, 361–380 (2015).

37 Serp, P. Carbon. *Comprehensive Inorganic Chemistry II (Second Edition): From Elements to Applications* **7**, 323–369 (2013).

38 Ayiania, M., Weiss-Hortala, E., Smith, M., McEwen, J. S. & Garcia-Perez, M. Microstructural analysis of nitrogen-doped char by raman spectroscopy: Raman shift analysis from first principles. *Carbon* **167**, 559–574 (2020).

39 Bousse, L. *et al.* Zeta potential measurements of ta2o5 and sio2 thin films. *Journal of Colloid and Interface Science* **147**, 22–32 (1991).

40 Tzounis, L. *et al.* Controlled growth of ag nanoparticles decorated onto the surface of sio2 spheres: a nanohybrid system with combined sers and catalytic properties. *RSC Advances* **4**, 17846–17855 (2014).

41 Krauskopf, K. B. Dissolution and precipitation of silica at low temperatures. *Geochimica et Cosmochimica Acta* **10**, 1–26 (1956).

Research outputs

On the basis of this thesis we have had a poster contribution at a conference. Furthermore, a paper is under preparation.

Supplementary information

Table S1: Overview table of the synthesis compositions conducted during this research.

Sample name	Citric acid (g)	Urea (mg)	Resazurin (mg)	Temperature (°C)	Solvent (10 ml)	Reaction time (H:MM)
CU180-H_2O	1000	2000	-	180	Water	3:00
CU250-R	20	40	20	250	-	0:15 min
CU250	1000	2000	-	250	-	0:15 min
CU180-GLY	1000	2000	-	250	Glycerol	0:15 min
CU180-FA	1000	2000	-	180	Formamide	3:00

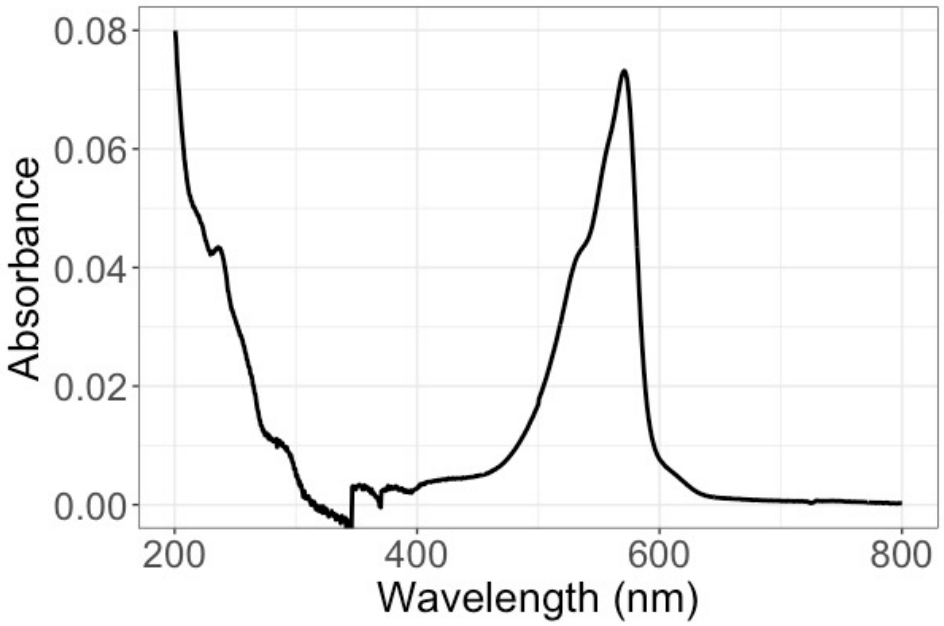

Figure S1: UV-vis spectrum of resorufin solution in water. Absorbance peak at 571 nm.

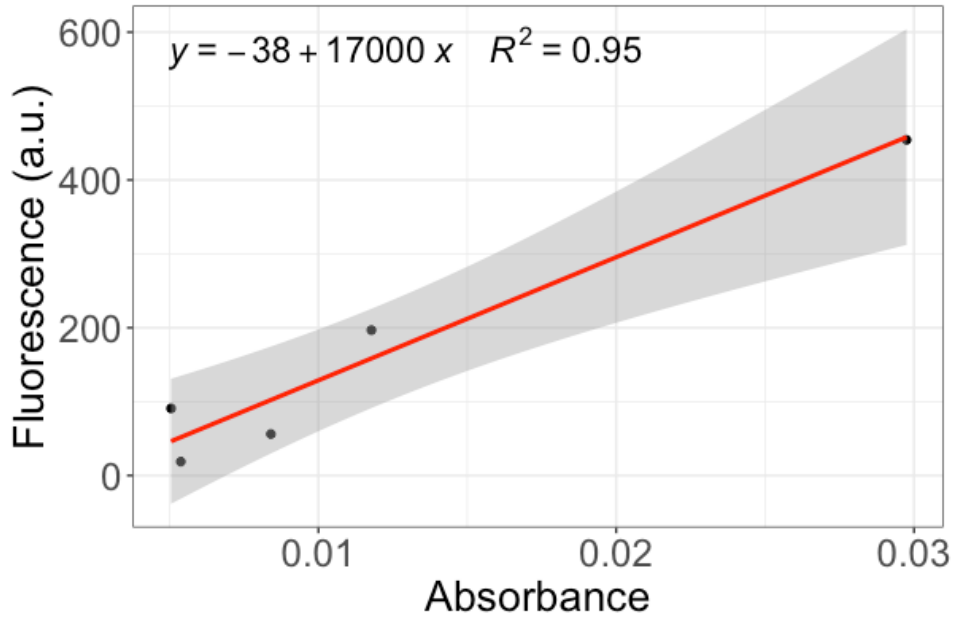

Figure S2: Absorbance vs fluorescence plot of different concentration samples of Rhodamine B for relative quantum yield calculations.

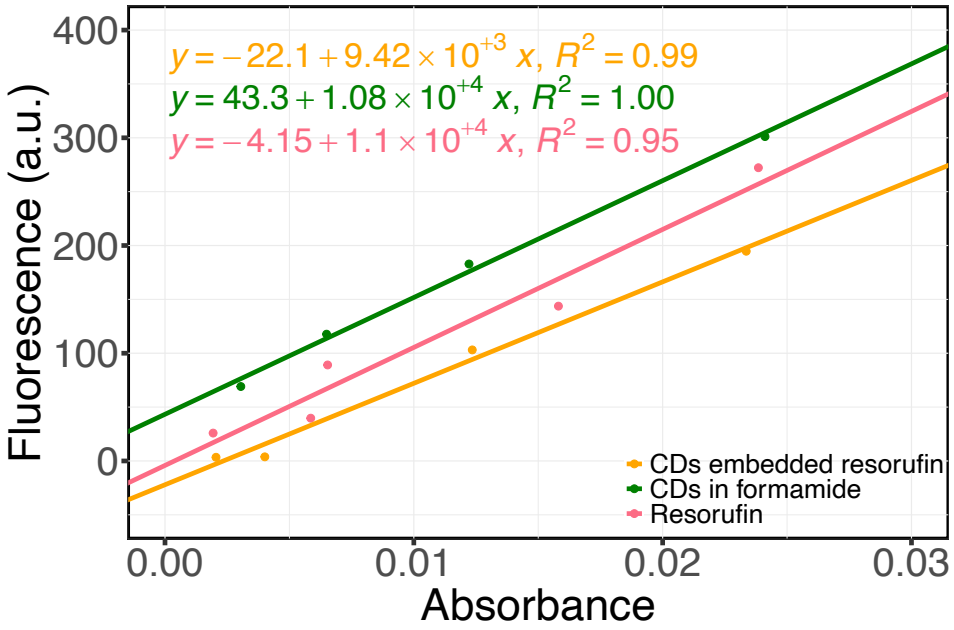

Figure S3: Absorbance vs fluorescence plot of different concentration samples of CDs with embedded resorufin (CU250-R, CDs prepared in formamide (CU180-FA), and resorufin. Data for relative quantum yield calculations.

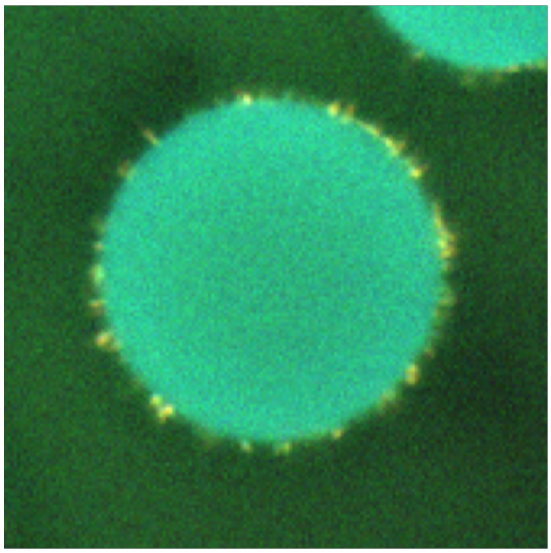

Figure S4: CSLM image of a single porous silica particle stained with CDs under a 0.01M NaCl condition.

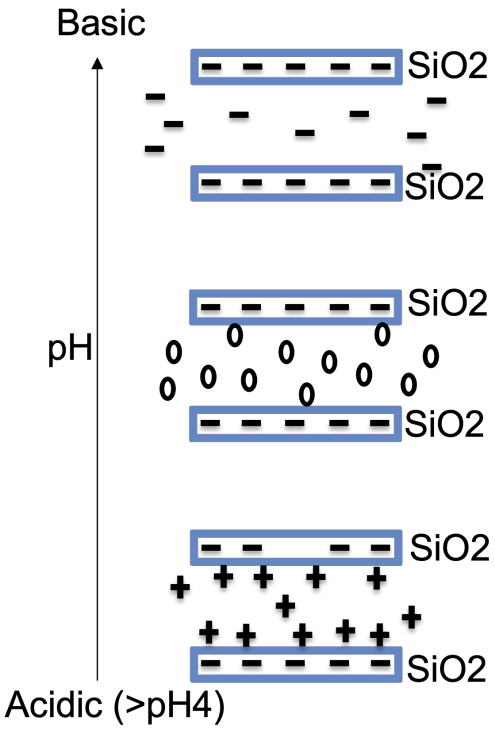

Figure S5: Schematic representation of the roughly expected electrostatic state and interactions of silica pore walls and CD particles at different pH values.

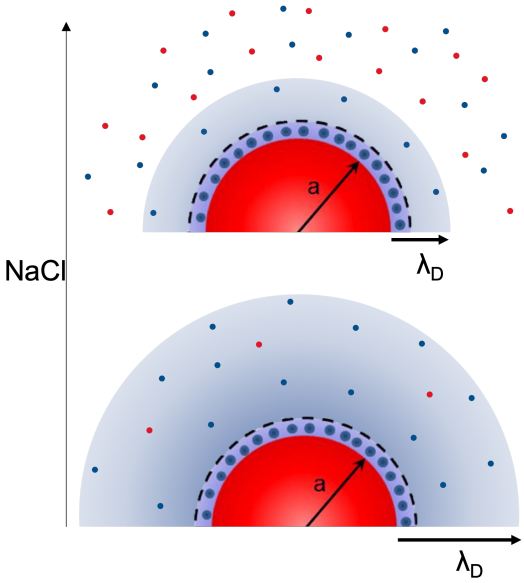

Figure S6: Schematic image of decreasing debye length with increasing salt concentration.